UNIVERSITYOF BIRMINGHAM

Elemental segregation and subsequent precipitation during solidification of continuous cast Nb–V–Ti high-strength low-alloy steels

Zheng, Shuguo; Davis, Claire; Strangwood, Martin

Accepted Manuscript

Elemental segregation and subsequent precipitation during solidification of continuous cast Nb–V–Ti high-strength low-alloy steels

Shuguo Zheng, Claire Davis, Martin Strangwood

Please cite this article as: Zheng Shuguo, Davis Claire, Strangwood Martin, Elemental segregation and subsequent precipitation during solidification of continuous cast Nb–V–Ti high-strength low-alloy steels, *Materials Characterization* (2014), doi: 10.1016/j.matchar.2014.06.008

Elemental segregation and subsequent precipitation during solidification of continuous cast Nb-V-Ti high-strength low-alloy steels

Shuguo Zheng[a], Claire Davis[b], Martin Strangwood[b]

([a]School of Materials and Metallurgy, Northeastern University, Shenyang 110819, P.R.China, E-mail: zhengsg@smm.neu.edu.cn, Tel: +86 24 83681496, Fax: +86 24 23906316; [b]Department of Metallurgy and Materials, University of Birmingham, Edgbaston, Birmingham, B15 2TT, UK)

ABSTRACT: In this study, elemental segregation during solidification and subsequent precipitation behaviour in a continuous cast Nb-V-Ti high-strength low-alloy steel was investigated by optical microscopy, scanning electron microscopy with energy dispersive X-ray spectroscopy and thermodynamic modeling. It is known that for steels with low carbon contents the pearlite that forms on slow cooling does so where the interdendritic liquid was present prior to final solidification. The alloying elements of Nb, Ti, Mn and V segregate into the interdendritic liquid during solidification, while Al preferentially segregates into the solidifying solid phase. The composition analysis on the slab samples verified the predicted element segregation behaviour, with a smaller difference in the concentrations of Mn and V in the pearlite and dendritic ferrite regions being observed compared to the Nb levels. Small (30-100 nm) spherical or irregular shaped Nb-rich precipitates (Nb(C, N) and (Nb, V)(C, N)) were mainly found in the pearlite regions, while angular Al-rich (60-300 nm) precipitates were found in the dendritic ferrite regions, in the form of AlN and complex AlN-V(C, N) precipitates. Small isolated ferrite regions surrounded by pearlite were observed in the microstructure and has two origins: one type is dendritic ferrite that appears as an isolated island due to a sectioning effect when observing the two-dimensional microstructure; the other is a

ferrite idiomorph that forms in the interdendritic region due to the low carbon content of the steel. Accordingly, in these isolated ferrite islands two different precipitation behaviours are found; predominantly Al-rich particles in the dendritic regions or predominantly Nb-rich precipitates in the interdendritic ferrite idiomorphs. No Al-rich precipitates were observed in the interdendritic regions (pearlite or isolated ferrite idiomorphs) despite the Thermo-Calc predictions indicating a higher volume fraction of AlN in these regions compared to the dendritic regions. This is believed to be due to back diffusion of nitrogen after solidification reducing the available nitrogen, which reacts with the high Nb levels present.

1. Introduction

High-strength low-alloy (HSLA) steels represent a group of low carbon steels that utilize small amounts of alloying elements to attain high strength and good toughness [1-4]. Microalloying elements, such as Nb, V and Ti, can facilitate grain refinement through precipitation in austenite and acting as grain boundary pinning particles during reheating, and/or can contribute to dispersion hardening through strain induced precipitation during rolling or through fine scale precipitation after the $\gamma \rightarrow \alpha$ transformation [5]. It is important that the segregation and precipitation behaviour in these steels is understood to allow for the successful design of the alloys and the optimum thermomechanical treatments to be adopted in order to achieve the desired mechanical properties. Nb, V and Ti are the most commonly added microalloying elements, although Al is often present in these steels as a result of the steel making process. The combined addition of these microalloying elements can lead to the formation of complex carbonitride precipitates (which contain at least two metallic elements), since the binary carbides and nitrides of Nb, V, Ti are

mutually soluble because of their B1 type structure [6,7]. Furthermore, the carbonitrides may also precipitate along with MnS or AlN particles [1,8,9].

Many investigations have been carried out to study the precipitation behaviour during the reheating or/and rolling process of microalloyed HSLA steels [5,8-19]. In those steels, precipitates forming during, or just after, solidification following continuous casting influence grain growth during the slab reheating process, and the solute distribution (resulting from precipitate dissolution during reheating, which is affected by segregation during solidification) affects the local recrystallisation and recovery processes during rolling [11]. In contrast to the wealth of data available for the particle dissolution and precipitation behaviour during the reheating and rolling processes in these steels, studies on the precipitation behaviour and distribution following solidification of continuous cast slabs are relatively scarce. Several studies [5,9,11-13] have been carried out to characterize precipitation in the interdendritic (predominantly pearlite in the final slab microstructure) and dendritic (ferrite in the final slab microstructure) regions of as-cast slab, but few investigations [12] pay attention to the precipitation behaviour in any isolated ferrite islands, which are surrounded by pearlite. The types of precipitates that form in these isolated ferrite islands is still not clear.

Segregation during steel solidification has been predicted by many models with different assumptions and simplifications [20-24]. However, these models are generally limited in considering segregation up to the end of solidification. A recent development has been to take into account segregation during solid state transformation to predict the final solute distribution [25,26]. A comprehensive understanding of the precipitation behaviour in the interdendritic and dendritic regions (including isolated ferrite islands) following solidification in microalloyed HSLA steels is essential to achieve the desired properties in the

final rolled plate. In the present work, elemental segregation during solidification and subsequent

precipitate characteristics (morphology and composition) in the pearlite and ferrite (dendritic and isolated

ferrite regions) of continuous cast Nb-V-Ti HSLA steels have been assessed and discussed.

2. Experimental

A continuous cast Nb-V-Ti HSLA slab measuring 290 mm thick and 1800 mm wide was investigated in

this study. The chemical composition of the slab is listed in Table 1. 15×10×10-mm samples were taken

from the subsurface (20 mm from the surface of the slab) and quarter width position as shown in Fig. 1.

Longitudinal sections were mounted in bakelite, polished to a 0.05 μm SiO_2 finish and etched in 2% nital

solution. These specimens were examined using a Zeiss Axioskop 2 microscope to quantify microstructure

features, such as the secondary dendrite arm spacing (SDAS) and fraction of pearlite. Precipitates were

characterized in a Jeol 7000 SEM equipped with Oxford Inca EDS facility. Thermodynamic modeling was

carried out using Thermo-Calc software version S with the TCFe7 database.

3. Results and Discussion

3.1. As-cast Microstructure and Cooling Rate

The microstructure of the continuous cast slab is shown in Fig. 2 and consists of light grey ferrite and dark

grey pearlite phases. The ferrite shows a dendritic morphology, reflecting formation in the dendritic regions

that were the original delta ferrite dendrites formed on solidification, whilst the pearlite is located at the

previously interdendritic areas. In addition, some isolated ferrite islands (ferrite totally surrounded by

pearlite) are observed inside the pearlite regions, as indicated in Fig. 2. These isolated ferrite regions may

be dendritic ferrite due to a sectioning effect or from ferrite idiomorphs forming in the interdendritic area.

The pearlite area fraction is 18.14±0.5% and the isolated ferrite area fraction is 0.28±0.05%.

It is known that the SDAS can be used to predict the cooling rate of the slab and investigators [20] have shown that, for low carbon steel ([C] ≤ 0.15 wt.%), the relationship is:

$$\lambda_{\text{SDAS}} = (169.1 - 720.9C_0)C_R^{-0.4935} \qquad (1)$$

Where λ_{SDAS} is the secondary dendrite arm spacing (μm), C_0 is the carbon content (wt.%), and C_R is the cooling rate (°C/s).

Fig. 3 shows the typical SDAS in the continuous cast slab and the measured average λ_{SDAS} is 117±15 μm based on 120 measurements, hence the estimated cooling rate for the slab during solidification is about 0.68 °C/s. It should be pointed out that the measured mean SDAS value could be broader than its actual value during cooling since the secondary arms become ever larger as the distance from a dendrite tip increases toward the base of a dendrite and the measured value represents the after-solidification state. So the actual cooling rate may be faster than the estimated value of 0.68 °C/s.

3.2. Prediction of Solidification Sequence, Element Segregation and Precipitation Behaviour

Thermo-Calc software was used in this study to predict the solidification sequence, element partition ratios and precipitation behaviour for the slab. The equilibrium solidification sequence with critical temperatures is shown in Fig. 4. It can be seen that, during cooling, δ-ferrite is predicted to form first from the liquid at 1517.7 °C and then a peritectic reaction takes place at 1486.7 °C, resulting in a temperature range where mixed liquid, δ-ferrite and austenite coexist with liquid disappearing at 1482.5 °C. Finally, the slab is fully transformed to austenite at 1475.2 °C. During solidification after the peritectic temperature, austenite will heterogeneously nucleate at the δ/liquid interface, therefore, the interdendritic liquid at the peritectic temperature becomes solute-enriched austenite grains and finally transforms to the pearlite (pearlite and idiomorphic ferrite) regions.

5

Table 2 shows the main parameters for the peritectic and eutectoid reactions predicted by Thermo-Calc. It can be seen that the liquid volume fraction at the peritectic temperature is almost equal to the predicted pearlite volume fraction in the slab, which suggests that the final pearlite forms at the same place as the original residual liquid at the peritectic temperature for the slab. In previous work [26] it has been suggested that when austenite forms at the peritectic temperature it provides a low diffusivity barrier layer, hence the interdendritic element segregation that occurs during the $L{\rightarrow}\delta$ transformation is effectively retained and is still present in the pearlite that forms. Therefore the dendritic element segregation is also mostly retained and is present within the dendritic ferrite. It has also been reported that additional compositional changes (for Mn) can occur during cooling through the austenite field (slightly) and diffusional transformation from austenite to ferrite (mostly) [25]. However, Nb, Ti, V and Al tend to form precipitates in the single phase austenite field prior to transformation to ferrite and so diffusion will be limited so that their segregated compositions are likely to closely reflect the as-just solidified condition. By comparing the experimentally measured (18.14%) and predicted pearlite fractions, it can be seen that there is around 5.45% difference in those data, with more pearlite being measured than predicted to form. This difference may be due to non-equilibrium cooling of the slab in the solid state.

In order to have a better understanding of the segregation behaviour, the predicted equilibrium partition coefficients (k) of solute elements for the slab are given in Table 3. The partition coefficient for elements of C, P, S, Nb, Ti, N are all less than 0.3 and that for elements of Mn and V are around 0.7, i.e. they prefer to segregate into the interdendritic area and therefore will be present preferentially in pearlite in the final microstructure. On the contrary, Al has a larger partition coefficient of around 1.26, so it will segregate into the solidifying δ-ferrite dendrite and finally be preferentially present in α-ferrite. It is to be pointed out that the partition coefficient for Al is larger than unity, which has also been found in previous investigations

6

[9,13].

Fig. 5 shows the predicted precipitation behaviour of various precipitates with temperature in the interdendritic and dendritic regions; predictions were made using the compositions of these regions at the peritectic temperature. The amounts of MnS and Ti-rich precipitates that are predicted to form are small due to the very low contents of S and Ti in the steel respectively. With decreasing temperature, Nb-rich precipitates are formed first followed by AlN and V-rich precipitates in the interdendritic regions, while AlN precipitates are formed first followed by Nb-rich and V-rich precipitates in the dendritic regions. Interdiffusion of Ti, V and Nb is predicted to occur in the Ti-rich, V-rich and Nb-rich precipitates, with the predominantly Ti-rich precipitates disappearing at 949 °C in the interdendritic regions and 817 °C in the dendritic regions, however, the elements of Ti, Nb and V in the precipitate are transferred into the V-rich and Nb-rich precipitates at lower temperatures. It is interesting to note that the volume fraction of AlN formed in the interdendritic region is predicted to be higher than that formed in the dendritic region, despite the predicted preferential segregation of Al into the ferrite (i.e. dendritic region). This is due to the significant predicted segregation of N into the interdendritic region and the formation of AlN being N limited, rather than Al limited, in the dendritic region.

Changes in the predicted equilibrium volume fractions of the precipitates can also be observed when phase transformations or new precipitates form during cooling. For example, the volume fractions of AlN and Nb-rich precipitates start to decrease at 774 °C in the dendritic regions, while a very small decrease of volume fraction of Nb-rich precipitates begins from 1049 °C in the interdendritic regions. Since the V-rich precipitates begin to form at these two temperatures for the dendritic and interdendritic regions respectively, as shown by Fig. 5, the decrease in volume fractions of AlN and Nb-rich precipitates may be due to the

7

formation of V(C, N), which is preferentially taking some of the nitrogen. The decrease in the volume

fraction of V-rich precipitates begins from 702 °C and 679 °C in the interdendritic and dendritic regions at

which temperatures cementite also starts to form, therefore some carbon in the V-rich precipitates may be

transferred into the cementite, resulting in the decrease in the volume fraction of V-rich precipitates.

3.3. Precipitation Characteristics

3.3.1. Precipitate Characteristics in Pearlite

It has been predicted from the partition coefficient values that the concentrations of Nb, Ti, Mn and V

should be higher in pearlite. In this study, spherical or irregular Nb-rich precipitates, with a size of 30-100

nm appearing as single precipitates or as clusters, were observed to form in pearlite, see Fig. 6(a). Most of

these particles are Nb(C, N) (Fig. 6(b)), with the other particles found to be complex (Nb, V)(C, N), see Fig.

6(c). No Nb-rich particles were observed in the dendritic ferrite regions. Ti-rich, MnS and V-rich

precipitates have not been found in the samples. The weight percentages of Ti and S in the steel are very

small (both are reported as 0.001 wt %) hence a very low number density of these precipitates is expected,

whilst V-rich precipitates are expected to be too small to be detected by the present SEM study.

Despite the Thermo-Calc predictions indicating a higher volume fraction of AlN in interdendritic regions

(pearlite or isolated ferrite idiomorphs) compared to the dendritic regions, no Al-rich precipitates were

observed in these regions. The possible reason will be discussed in detail in the following section 3.4.

3.3.2. Precipitate Characteristics in Dendritic Ferrite

An inhomogeneous distribution of precipitates was observed in the dendritic ferrite regions. Particles with a

size of 60 to 300 nm appeared as single precipitates, in clusters, or sometimes along the prior austenite

grain boundaries, see Fig. 7(a). Thermo-Calc predicts enrichment of Al in the delta ferrite during

solidification, and V is also expected to be present in dendritic ferrite, due to its partition coefficient being

0.73 (relatively weak tendency to segregate). EDS analysis has shown the presence of Al in the irregular shaped particles, Fig. 7(b), with V also being detected in some precipitates, Fig. 7(c). The majority of the particles are AlN, with the presence of V being consistent with some V(C, N) precipitates nucleating on pre-existing AlN particles, resulting in the complex AlN-V(C, N) precipitates in dendritic ferrite. No Nb or Ti has been detected in these Al-rich particles, and Nb-rich precipitates have not been found in the dendritic ferrite regions.

3.3.3. Precipitate Characteristics in Isolated Ferrite Islands Surrounded by the Pearlite

Isolated ferrite islands inside the pearlite regions have been observed. As mentioned above, these isolated ferrite islands may be from dendritic ferrite due to a sectioning effect when viewing a two-dimensional microstructure, or from ferrite forming in the interdendritic area. Two different types of precipitation behaviour in these isolated ferrite islands were observed, i.e. isolated ferrite islands with either Al-rich or Nb-rich precipitates were detected as shown by Fig. 8 and Fig. 9 respectively. Table 4 shows the measured weight percent of Mn in the matrix of the isolated ferrite islands with Al-rich or Nb-rich particles (shown in Fig. 8 and Fig. 9) and in the surrounding pearlite and dendritic ferrite. It can be seen that the pearlite has a higher matrix Mn level than the dendritic ferrite, consistent with the predicted segregation of Mn into interdendritic liquid during solidification. The isolated ferrite island with Al-rich precipitates has almost the same matrix Mn level as the nearby dendritic ferrite, which means that this kind of isolated ferrite island is also dendritic ferrite, appearing in the pearlite due to the sectioning effect. Therefore Al-rich precipitates exist in these isolated ferrite islands as expected in dendritic ferrite. It can also be seen from Table 4 that the matrix Mn level in the isolated ferrite island with Nb-rich precipitates is similar to that in the surrounding pearlite (both are higher than that in the nearby dendritic ferrite), indicating that this isolated ferrite region may be a ferrite idiomorph forming in the interdendritic region.

9

In the ferrite idiomorphs forming in the interdendritic region, spherical or irregular Nb-rich precipitates with a size of 50-300 nm were detected and they appear as single precipitates or as clusters, see Fig. 9(a). Most of these particles are Nb(C, N) (Fig. 9(b)), with the other particles being found to be complex (Nb, V)(C, N), see Fig. 9(c). To have a better understanding of the precipitation behaviour in these ferrite idiomorphs, a comparison of precipitation behaviour in dendritic ferrite (339 particles and 2373 μm^2 total area analysed in the center region of dendrite ferrite adjacent to the isolated ferrite island shown by Fig. 9) and interdendritic isolated ferrite (39 particles and 581 μm^2 total area analysed from the whole isolated ferrite island shown by Fig. 9) is listed in Table 5, and the precipitate size distributions in these two regions are also shown in Fig. 10. Furthermore, to compare the predicted and observed precipitate number densities in dendritic ferrite and interdendritic isolated ferrite, the predicted volume fractions of AlN for dendritic and Nb-rich carbonitrides for interdendritic regions as well as the measured average precipitates sizes in these two regions were used to calculate the predicted precipitate number densities and the results are also listed in Table 5. It can be seen that, forming in the interdendritic region, the interdendritic isolated ferrite has similar precipitation behaviour to the pearlite region. The precipitates in interdendritic isolated ferrite have larger average size but smaller number density than those in dendritic ferrite. In addition the particle sizes showed a wider, more normal distribution in interdendritic isolated ferrite than in dendritic ferrite, which tended to have a more narrow distribution skewed to large sizes. By comparing the experimental and predicted precipitate number densities, it can be seen that the predicted one is very close to the measured one in the interdendritic isolated ferrite, while the predicted one is a bit smaller than the measured one in the dendritic ferrite (but in the same order of magnitude). In addition, the precipitate number density in dendritic ferrite is larger than that in the interdendritic isolated ferrite for the experimental results, while they are the same for the predicted results.

3.4. Discussion

By using the compositions in the interdendritic and dendritic regions at the peritectic temperature, the precipitation behaviour in these regions have been predicted, as shown by Fig. 5 with the predicted temperatures for transformation to complete austenite and start of formation of typical precipitates given in Table 6. As discussed above, these predictions do not match well with the experimental observations as AlN was seen in the dendritic regions but no AlN particles were found in the interdendritic regions despite the predictions giving a large volume fraction in the interdendritic regions. It can be seen that AlN and Nb-rich precipitates are predicted to form in full austenite in the interdendritic and dendritic regions. Considering that the interstitial elements (C, N) can diffuse rapidly in austenite, whilst the substitutional elements will have low diffusivity, and that there will be a driving force to homogeneous the material, it is reasonable to consider the steel, at these temperatures, to have a more uniform C and N composition. Therefore the compositions of substitutional elements in the interdendritic and dendritic regions at the peritectic temperature and the average slab compositions of C and N were also used to predict the precipitation behaviour of the various precipitates with temperature in these regions, shown by Fig. 11 and listed in Table 6.

It can be seen from Figs. 5 and 11 that, when predictions are made with the average slab compositions of C and N, the precipitation temperatures of AlN, Nb-rich and V-rich are all decreased by over 100 °C and the maximum volume fraction of AlN changed from 0.082% to 0.055% for the interdendritic regions. While the precipitation temperatures of AlN, Nb-rich and V-rich all increased by less than 35 °C and the maximum volume fraction of AlN changed from 0.043% to 0.055% for dendritic regions. It can also be seen from Fig. 11 that, although the maximum volume fractions of AlN are the same for the interdendritic and dendritic regions, the precipitation temperature of AlN in the dendritic region is 102 °C higher than that

in interdendritic regions. It might be expected that this would result in larger AlN particles being seen in the dendritic regions. Furthermore, the temperature when the volume fraction of AlN reaches 0.050% is 881 °C in the dendritic region, while it is 676 °C in interdendritic region, suggesting that any AlN that forms in the interdendritic region will be smaller than in the dendritic region, which may explain why no AlN is observed in the interdendritic area. It seems that, by using the average slab compositions of C and N as well as the compositions of substitutional elements in the interdendritic and dendritic regions at the peritectic temperature, the predicted results are more consistent with the experimental results. Furthermore, when predicting using the average slab compositions of C and N, the predicted precipitates number densities in dendritic ferrite and interdendritic isolated ferrite are 5.2×10^4 and 4.3×10^4 number/mm^2 respectively, by using the measured average precipitates sizes in these two regions (shown in Table 5) as well as the predicted volume fractions of AlN for dendritic and Nb-rich for interdendritic regions. These results give better agreement with the experimental results in that the precipitate number density in the dendritic ferrite is larger than that in the interdendritic isolated ferrite.

4. Conclusions

The distribution, size and type of precipitates in a continuous cast Nb-V-Ti high-strength low-alloy (HSLA) steel slab have been measured. In particular the different microstructural regions of dendritic ferrite and interdendritic pearlite have been characterised, with isolated ferrite regions within the pearlite also being assessed. In addition Thermo-Calc predictions for segregation and precipitate type have been made. It was found that:

SEM-EDS analysis on the slab samples was consistent with the predicted element segregation behaviour during solidification. Small spherical or irregular Nb-rich precipitates (Nb(C, N) and (Nb,V)(C, N)) were

mainly found in the pearlite regions, due to preferential segregation of Nb into the interdendritic area, while angular Al-rich precipitates were found in the dendritic ferrite regions, in the form of AlN and complex AlN-V(C, N) precipitates, due to preferential segregation of Al into the dendritic area.

Small isolated ferrite regions surrounded by pearlite were observed in the as-cast microstructure. Two different precipitation behaviours have been found due to different formation mechanisms of the isolated ferrite islands. One type of isolated ferrite island is dendritic ferrite, appearing in the pearlite due to a sectioning effect when observing a two-dimensional microstructure and it was observed that Al-rich precipitates exist in this form of isolated ferrite island. The other type is a ferrite idiomorph, with Nb-rich particles forming in the interdendritic region.

The precipitates in interdendritic isolated ferrite (Nb-rich type) have a larger average size but smaller number density than those in dendritic ferrite (Al-rich type). No Al-rich precipitates were observed in the interdendritic regions (pearlite or isolated ferrite idiomorphs) despite the Thermo-Calc predictions indicating a higher volume fraction of AlN predicted in these regions compared to the dendritic regions when making predictions using the composition in the interdendritic and dendritic regions at the peritectic temperature. The predictions were improved, giving better agreement to the observed precipitate distributions, when made using the segregated substitutional element compositions at the peritectic temperature but the average C and N compositions for the slab. This is consistent with complete back diffusion of highly mobile C and N in austenite before precipitation.

Acknowledgements

REFERENCES

[1] Skobir DA. High-strength low-alloy (HSLA) steels. Mater Tehnol 2011; 45: 295-301.

[2] Vervynckt S, Verbeken K, Lopez B, Jonas JJ. Modern HSLA steels and role of non-recrystallisation temperature. Int Mater Rev 2012; 57: 187-207.

[3] Show BK, Veerababu R, Balamuralikrishnan R, Malakondaiah G. Effect of vanadium and titanium modification on the microstructure and mechanical properties of a microalloyed HSLA steel. Mater Sci Eng A 2010; 527: 1595-604.

[4] Liu ZK. Thermodynamic calculations of carbonitrides in microalloyed steels. Scr Mater 2004; 50: 601-6.

[5] Jun HJ, Kang KB, Park CG. Effects of cooling rate and isothermal holding on the precipitation behavior during continuous casting of Nb–Ti bearing HSLA steels. Scr Mater 2003; 49: 1081-6.

[6] Loberg B, Nordgren A, Strid J, Easterling KE. The role of alloy composition on the stability of nitrides in Ti-microalloyed steels during weld thermal cycles. Metall Trans A 1984; 15: 33-41.

[7] Okaguchi S, Hashimoto T. Characteristics of precipitates and mechanical properties in Ti bearing HSLA steels. Trans ISIJ 1987; 27: 467-73.

[8] Craven AJ, He K, Garvie LAJ, Baker TN. Complex heterogeneous precipitation in titanium–niobium microalloyed Al-killed HSLA steels—II. Non-titanium based particles. Acta Mater 2000; 48: 3869-78.

[9] Chakrabarti D, Davis CL, Strangwood M. Development of bimodal grain structures in Nb-containing high-strength low-alloy steels during slab reheating. Metall Mater Trans A 2008; 39: 1963-77.

[10] Craven AJ, He K, Garvie LAJ, Baker TN. Complex heterogeneous precipitation in titanium–niobium microalloyed Al-killed HSLA steels—I. (Ti, Nb)(C, N) particles. Acta Mater 2000, 48: 3857-68.

[11] Davis CL, Strangwood M. Preliminary study of the inhomogeneous precipitate distributions in Nb-microalloyed plate steels. J Mater Sci 2002; 37: 1083-90.

[12] Kundu A, Davis CL, Strangwood M. Grain size distributions after single hit deformation of a segregated, commercial Nb-containing steel: prediction and experiment. Metall Mater Trans A 2011; 42: 2794-806.

[13] Davis CL, Strangwood M. Segregation behaviour in Nb microalloyed steels. Mater Sci Technol 2009; 25: 1126-33.

[14] Fernández J, Illescas S, Guilemany JM. Effect of microalloying elements on the austenitic grain growth in a low carbon HSLA steel. Mater Lett 2007; 61: 2389-92.

[15] Pereloma EV, Timokhina IB, Russell KF, Miller MK. Characterization of clusters and ultrafine precipitates in Nb-containing C–Mn–Si steels. Scr Mater 2006; 54: 471-6.

[16] Mishra SK, Ranganathan S, Das SK, Das S. Investigations on precipitation characteristics in a high strength low alloy (HSLA) steel. Scr Mater 1998; 39: 253-9.

[17] Charleux M, Poole WJ, Militzer M, Deschamps A. Precipitation behavior and its effect on strengthening of an HSLA-Nb/Ti steel. Metall Mater Trans A 2001; 32: 1635-47.

[18] Zhang QA, Zhang ZY, Jiao SH. Precipitates and hydrogen permeation in HSLA steel produced by TMCP. Corros Eng Sci Techn 2011; 46: 375-9.

[19] Poths RM, Higginson RL, Palmiere EJ. Complex precipitation behaviour in a microalloyed plate steel. Scr Mater 2001; 44: 147-51.

[20] Won YM, Thomas BG. Simple model of microsegregation during solidification of steels. Metall Mater

Trans A 2001; 32: 1755-67.

[21] Voller VR, Beckermann C. A unified model of microsegregation and coarsening. Metall Mater Trans A 1999; 30: 2183-9.

[22] Wang CY, Beckermann C. A unified solute diffusion model for columnar and equiaxed dendritic alloy solidification. Mater Sci Eng A 1993; 171: 199-211.

[23] Bower TF, Brody HD, Flemings MC. Measurements of solute redistribution in dendritic solidification. Trans Met Soc AIME 1966; 236: 624-33.

[24] Clyne TW, Kurz W. Solute redistribution during solidification with rapid solid state diffusion. Metall Trans A 1981; 12: 965-71.

[25] Strangwood M, Zhang DY, Davis CL. A comparison of analytical and calphad-based modelling for simulation of segregation during casting of steels. E-Proceedings of Science and Technology of Ironmaking and Steelmaking (STIS 2013); 2013.

[26] Zhang DY, Strangwood M. Characterisation and modelling of microsegregation in low carbon continuously cast steel slab. Proceedings of the 2013 International Symposium on Liquid Metal Processing & Casting; 2013. p. 321-7.

Tables

Table 1 □ Chemical composition of the investigated slab (wt.%).

	C	Si	Mn	P	S	Ni	Al	Nb	V	Ti	N
Slab	0.10	0.28	1.41	0.013	0.001	0.30	0.029	0.027	0.050	0.001	0.008

Table 2 □ Main parameters for the peritectic and eutectoid reactions predicted by Thermo-Calc.

	Peritectic reaction parameters	Eutectoid reaction parameters
Reaction equation	$L+\delta\rightarrow\gamma$	$\gamma\rightarrow Fe_3C+\alpha_P$ [a]
Reaction temperature, °C	1486.7	685.0
Phase volume fraction, %	12.95 (Liquid phase at 1486.7 °C)	12.69 (P [b])

[a] α_P stands for α-ferrite in pearlite, [b] P stands for pearlite

Table 3 □ Predicted equilibrium partition coefficients of solute elements in the slab.

Element	C	Si	Mn	P	S	Ni	Al	Nb	Ti	N	V
k	0.15	0.63	0.68	0.29	0.02	0.79	1.26	0.19	0.25	0.29	0.73

Table 4 □ Measured weight percent of Mn in the matrix of the isolated ferrite islands with Al-rich or Nb-rich particles and in pearlite and dendritic ferrite (wt.%).

	Isolated ferrite island with Al-rich precipitates		Isolated ferrite island with Nb-rich precipitates	
	[Mn]	Average [Mn]	[Mn]	Average [Mn]
Isolated ferrite island	1.40-1.60	1.48	1.60-1.80	1.65
Dendrite center (dendrite located adjacent to isolated ferrite island)	1.40-1.60	1.50	1.40-1.60	1.51
Pearlite surrounding the isolated ferrite island	1.60-1.85	1.76	1.60-1.85	1.73

Table 5 □ Comparison of precipitation behaviour in dendritic ferrite and interdendritic isolated ferrite.

	Dendritic ferrite	Interdendritic isolated ferrite
Measured average precipitate size, nm	117.0	185.4
Measured precipitate number densities, $\times 10^4$ Number/mm²	14.3	6.7
Precipitate types	Al-rich (AlN, AlN-V(C, N))	Nb-rich (Nb(C, N), (Nb, V)(C, N))
Predicted precipitate volume fraction, $\times 10^{-4}$	4.3	11.0
Predicted precipitate number densities, $\times 10^4$ Number/mm²	4.0	4.0

Table 6 □ Predicted temperatures for transforming to complete austenite, start of formation of typical precipitates in the interdendritic and dendritic regions.

	Interdendritic regions	Dendritic regions
Temperatures for transforming to complete austenite, °C	1404	1453
Temperatures for start of formation of AlN precipitates (full segregated composition), °C	1154	1093
Temperatures for start of formation of AlN precipitates (segregated substitutional element and average C, N composition), °C	1016	1118
Temperatures for start of formation of Nb-rich precipitates (full segregated composition), °C	1391	1063
Temperatures for start of formation of Nb-rich precipitates (segregated substitutional element and average C, N composition), °C	1269	1096

Table captions

Table 1 □ **Chemical composition of the investigated slab (wt.%).**

Table 2 □ **Main parameters for the peritectic and eutectoid reactions predicted by Thermo-Calc.**

Table 3 □ **Predicted equilibrium partition coefficients of solute elements in the slab.**

Table 4 □ **Measured weight percent of Mn in the matrix of the isolated ferrite islands with Al-rich or Nb-rich particles and in pearlite and dendritic ferrite (wt.%).**

Table 5 □ **Comparison of precipitation behaviour in dendritic ferrite and interdendritic isolated ferrite.**

Table 6 □ **Predicted temperatures for transforming to complete austenite, start of formation of typical precipitates in the interdendritic and dendritic regions.**

Figure captions

Fig. 1 ☐ Schematic diagram of the location of samples in the slab (all dimensions in millimetres).

Fig. 2 ☐ Optical microstructure of the continuous cast slab.

Fig. 3 ☐ Typical SDAS in the continuous cast slab.

Fig. 4 ☐ Solidification sequence of Liquid (L), δ-ferrite (δ) and austenite (γ) with critical temperatures.

Fig. 5 ☐ The predicted precipitation behaviour of various precipitates with temperature in the interdendritic (a) and dendritic (b) regions using the compositions in these regions at the peritectic temperature.

Fig. 6 ☐ (a) SEM image showing the various distributions (single and cluster) and shapes (spherical and irregular) of Nb-rich precipitates observed in pearlite, (b) EDS spectrum of particle A showing the Nb peaks, (c) EDS spectrum of particle B showing Nb and V peaks.

Fig. 7 ☐ (a) SEM image showing the various distributions (single, cluster and along the prior austenite grain boundaries) of Al-rich precipitates in dendritic ferrite, (b) EDS spectrum of particle C showing Al peaks, (c) EDS spectrum of particle D showing Al and V peaks.

Fig. 8 ☐ The precipitation behaviour in isolated ferrite with Al-rich precipitates.

Fig. 9 ☐ (a) SEM image showing the various distributions (single and cluster) and shapes (spherical and irregular) of Nb-rich precipitates in isolated ferrite, (b) EDS spectrum of particle E showing Nb peaks, (c) EDS spectrum of particle F showing Nb and V peaks.

Fig. 10 ☐ Precipitate size distributions in (a) dendritic ferrite and (b) interdendritic isolated ferrite.

Fig. 11 ☐ The predicted precipitation behaviour of various precipitates with temperature in the interdendritic (a) and dendritic (b) regions using the substitutional element compositions in these

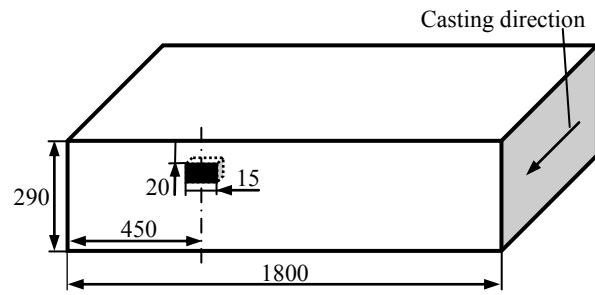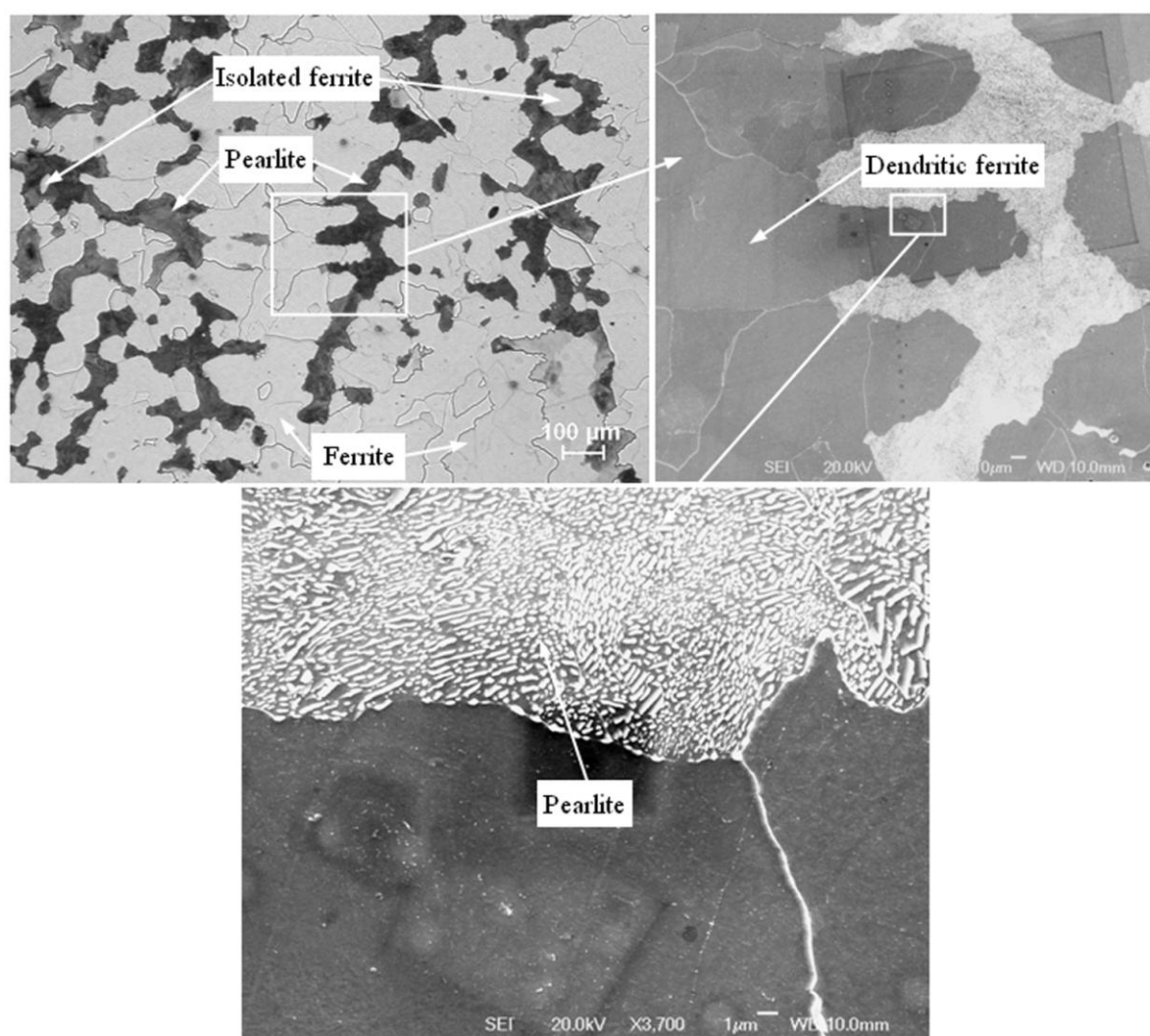**regions at the peritectic temperature and the average slab compositions of C and N.**

Figure 1

Figure 2

Figure 3

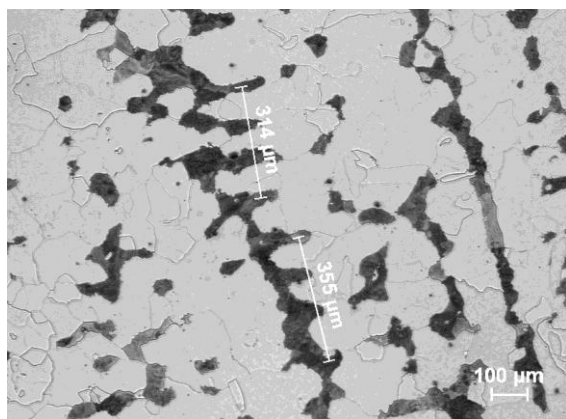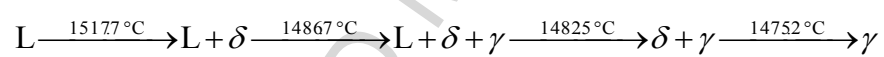$$L \xrightarrow{1517.7\,°C} L + \delta \xrightarrow{1486.7\,°C} L + \delta + \gamma \xrightarrow{1482.5\,°C} \delta + \gamma \xrightarrow{1475.2\,°C} \gamma$$
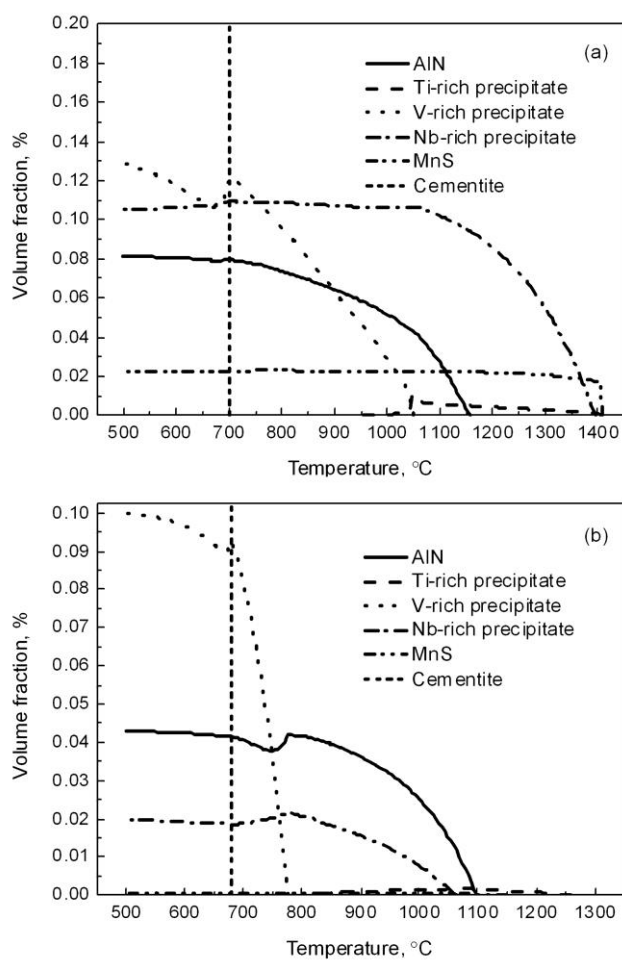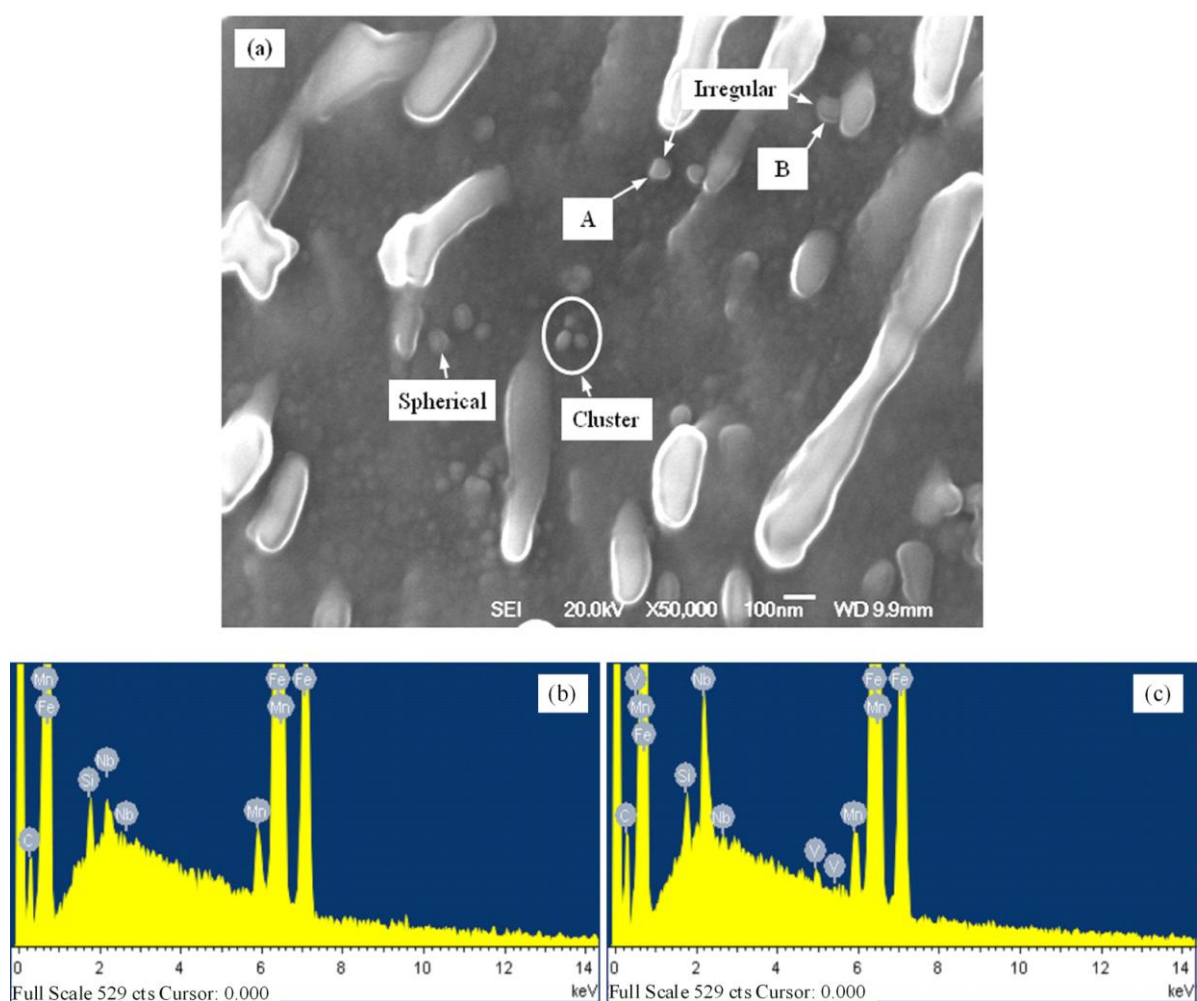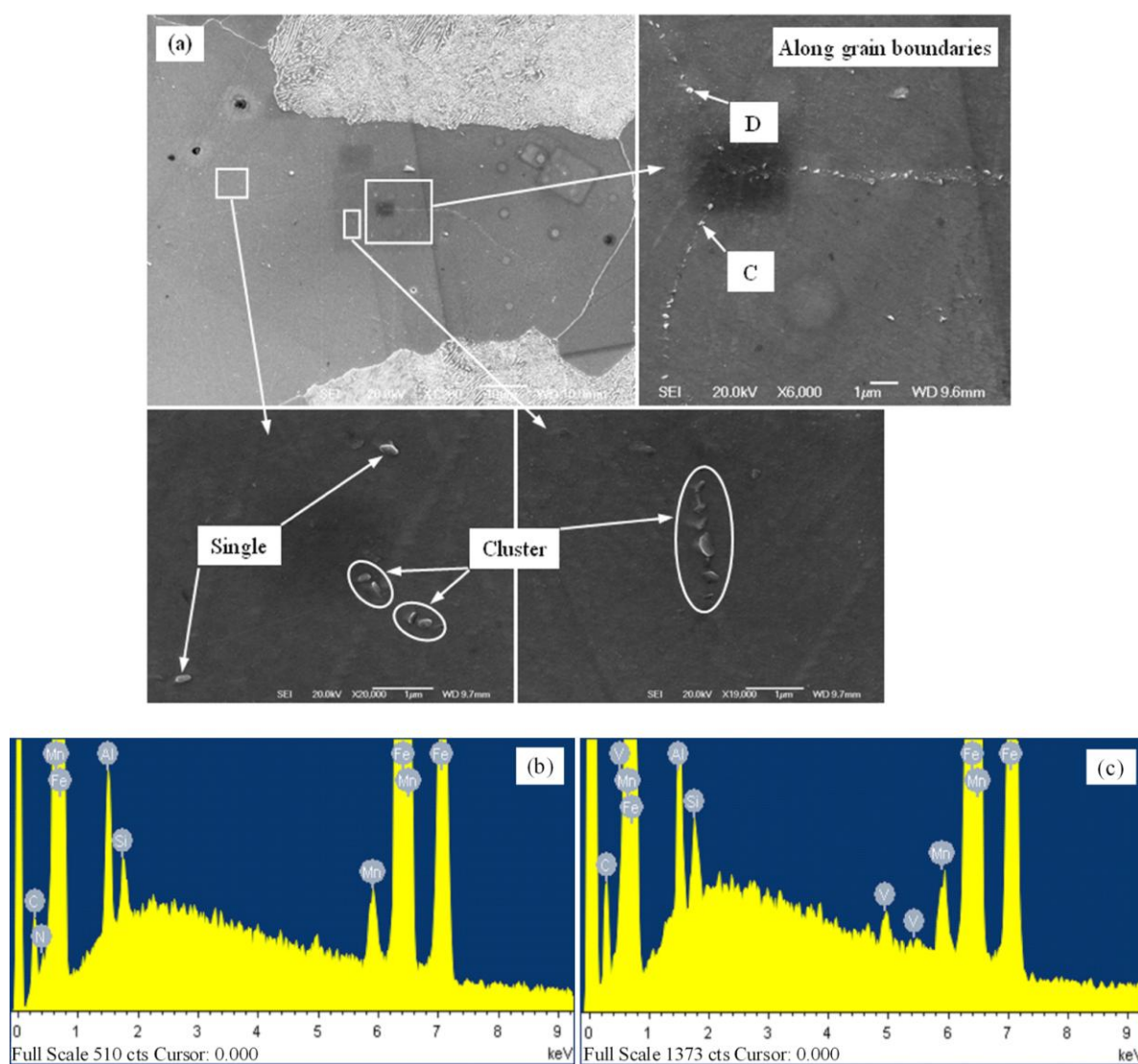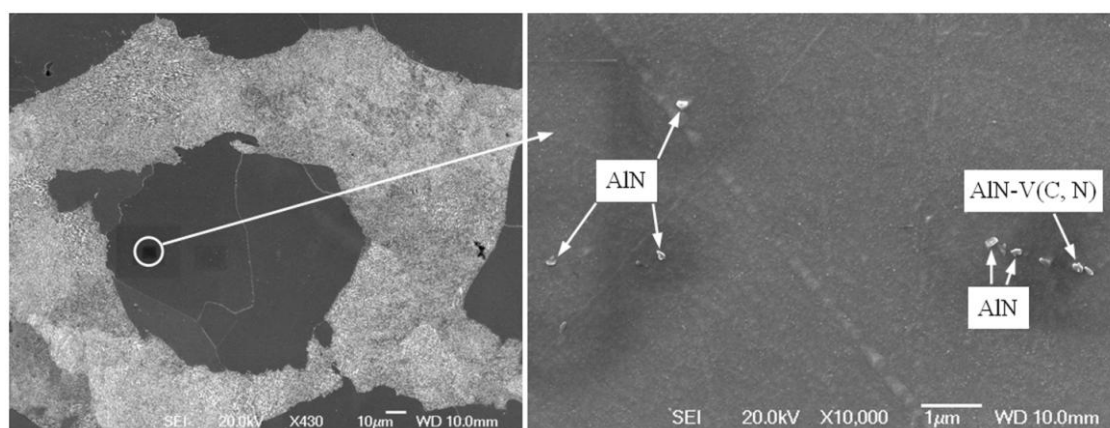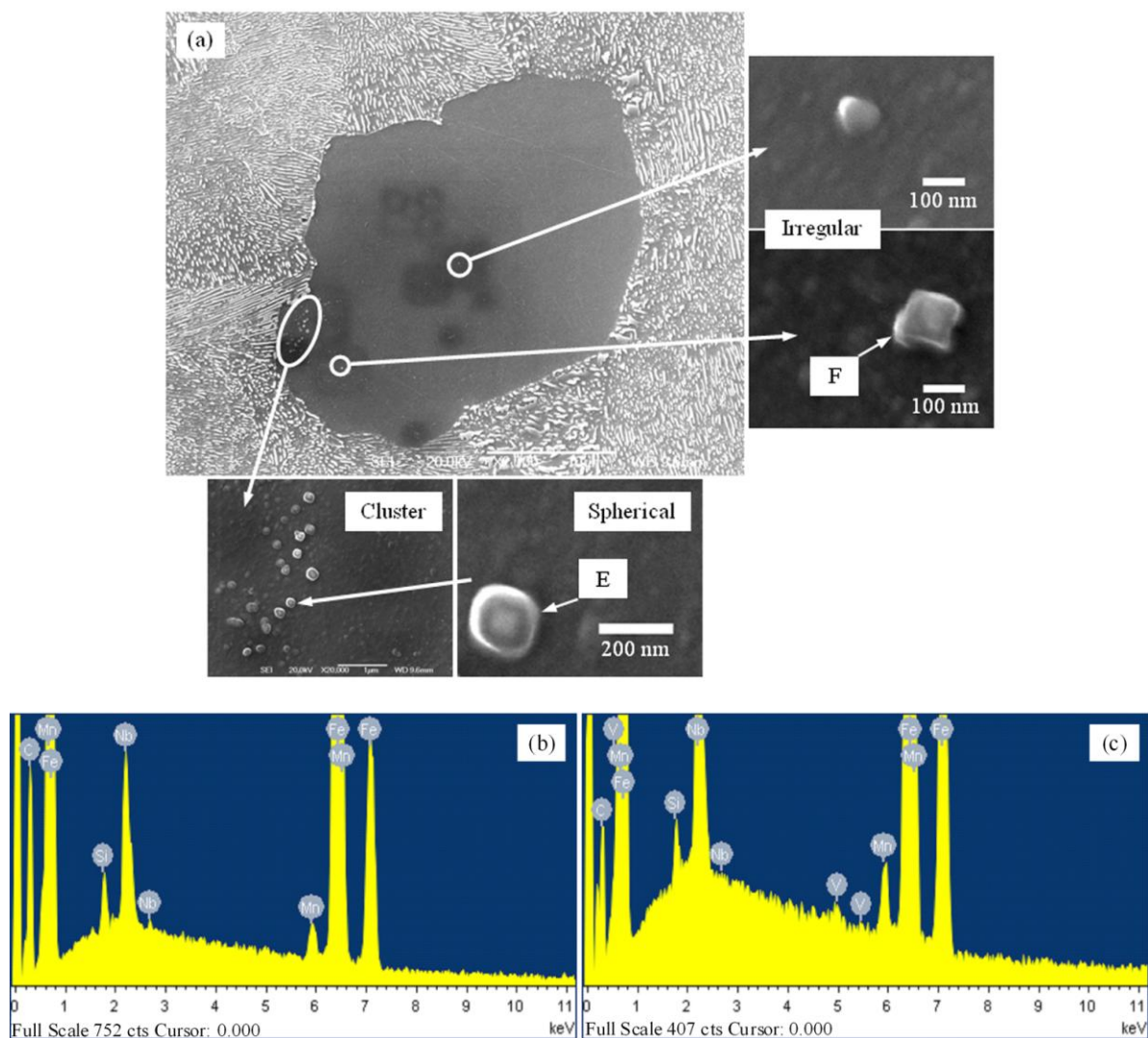
Figure 4

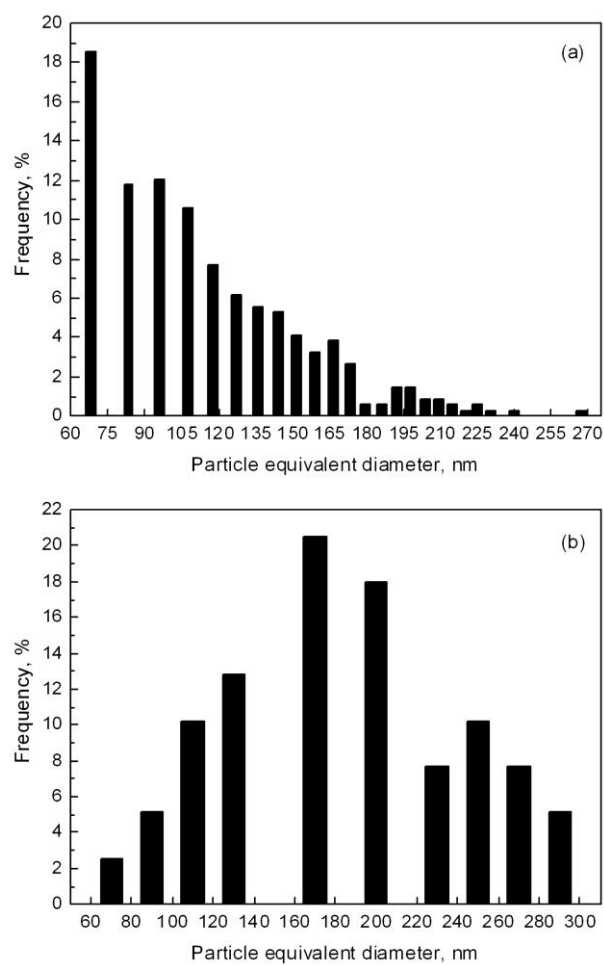Figure 5

Figure 6

Figure 7

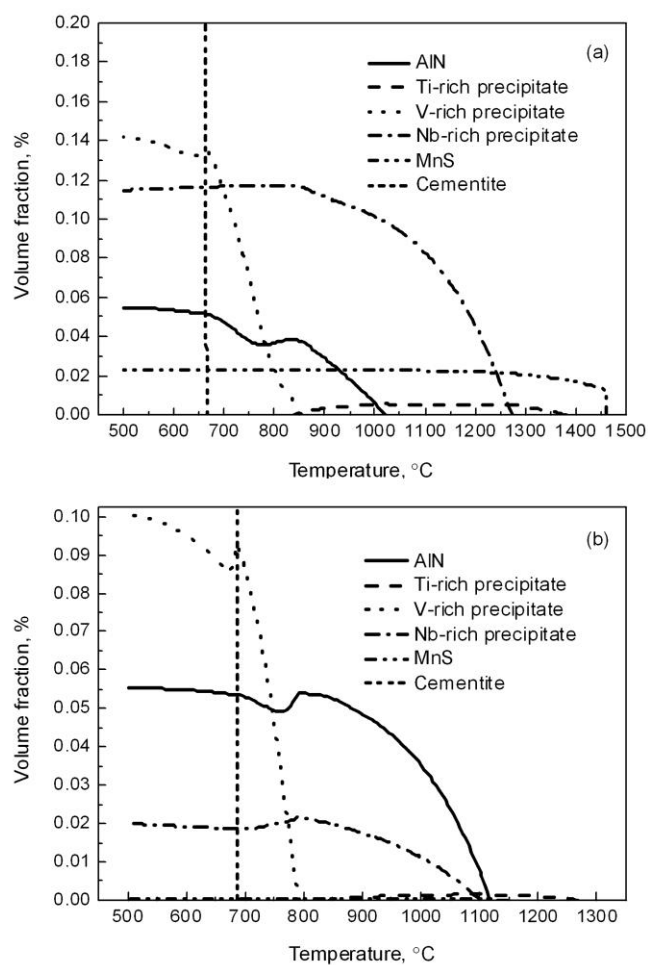Figure 8

Figure 9

Figure 10

Figure 11

32

Highlights

> ➢ Nb-rich precipitates (Nb(C, N) and (Nb,V)(C, N)) were mainly found in pearlite.
> ➢ Angular Al-rich precipitates (AlN and AlN-V(C, N)) were found in dendritic ferrite.
> ➢ Precipitation behaviour in isolated ferrite islands within pearlite was revealed.
> ➢ Segregation of substitutional elements during solidification is retained.
> ➢ Back diffusion of interstitial elements (C, N) occurred.